Adaptive optics system with micromachined mirror array and stochastic gradient descent controller

T. Weyrauch[a,c], M. A. Vorontsov[a], T. G. Bifano[b], and M. K. Giles[c]

[a)]U.S. Army Research Laboratory, Information Science and Technology Directorate, Adelphi, MD 20783
[b)]Boston University, Manufacturing Engineering Department, Brookline, MA 02446
[c)]New Mexico State University, Klipsch School for Electrical and Computer Engineering, Las Cruces, NM 88003

ABSTRACT

An adaptive laser beam focusing system comprising a 4×4 segment (5×5 actuator) MEMS deformable mirror developed at Boston University is presented. Mirror actuators were controlled by a circuit using VLSI chips implementing a stochastic parallel gradient descent algorithm. The system allowed for an enhancement of the iteration rate up to 5900 s^{-1}, limited only by the used computer equipment. Results of experiments for characterization of the MEMS mirror response and the adaptation speed of the system are reported. A further improvement of adaptation speed was achieved by modification of the control algorithm implementing a self-optimization of one parameter.

Keywords: adaptive optics, MEMS deformable mirror, model-free optimization, parallel gradient descent

1. INTRODUCTION

Current opto-electronic adaptive optics systems are usually based on wavefront measurements and phase compensation. Although this method is successfully implemented in astronomical applications[1], its application appears difficult in situations where wavefront distortions cannot be measured directly (e. g. in anisoplanatic imaging conditions) or where strong intensity modulation (scintillation) induces severe problems to wavefront measurements. Therefore model-free optimization has been considered as an alternative control strategy, which might be able to overcome these difficulties. This approach requires the definition of a single scalar system performance metric *J*, which may be considered as a function of the control parameters $\vec{u}$. An approximation of the gradient of *J* with respect to $\vec{u}$ can be obtained by application of perturbations to the control parameters and subsequent measurement of the metric perturbation. Following the gradient in several iterations until an *extremum* allows for optimization without any further knowledge of the system. However, straightforward gradient estimation by application of perturbations to all parameters sequentially is time consuming especially in the case of a large number of control channels. Another approach, recently adopted and modified for application in adaptive optics systems and known as stochastic parallel gradient descent technique improves the time required for gradient estimation on the cost of a somewhat worse approximation[2,3]. Perturbations are applied in parallel to all control channels and the metric perturbation is measured only once per iteration step. The faster convergence of the gradient approximation is obtained due to the selection of perturbations as statistically independent random variables. A major advantage of the stochastic parallel gradient descent algorithm is the possibility of its implementation in very large scale integrated parallel electronic circuits, as recently demonstrated in frames of a cooperation between the Army Research Laboratory and the Johns Hopkins University[4]. With the availability of a fast parallel controlling circuit (referred to as AdOpt VLSI controller) allowing for working rates in the order of 10^5 s^{-1}, attempts to improve the iteration rate of the whole adaptive optical system face the problem of the response time of the wavefront correcting elements. Piezoelectric driven deformable mirrors and liquid crystal phase modulators limit the working rate so far to the order of 100 s^{-1} or even less. The recent development of deformable mirrors based on MEMS technology induced a major improvement of the situation and a iteration rate of 1500 s^{-1} was recently reported[5].

In this paper we present results from a simple adaptive focusing system comprising the AdOpt VLSI controller as well as a fast MEMS deformable mirror developed at Boston University, which allowed for a further significant improvement of the iteration rate. Measurements for characterization of the mirror and the system performance are presented. An improvement of the control algorithm is discussed.

High-Resolution Wavefront Control: Methods, Devices, and Applications II, John D. Gonglewski, Mikhail A. Vorontsov, Mark T. Gruneisen, Editors, Proceedings of SPIE Vol. 4124 (2000) © 2000 SPIE. · 0277-786X/00/$15.00

2. STOCHASTIC PARALLEL GRADIENT DESCENT CONTROLLER

To use the parallel gradient descent algorithm in an adaptive optical system to control e. g. a deformable mirror, a system performance metric $J(\vec{u})$ depending on the set of voltages $\vec{u} = (u_1, \ldots, u_j, \ldots, u_N)$ applied to the mirror actuators must be defined. Each iteration step n of the algorithm begins with the selection of a set of perturbation voltages $\delta\vec{u} = (\delta u_1, \ldots, \delta u_j, \ldots, \delta u_N)$, following an Bernoulli distribution, i. e. the absolute values of all δu_j are identical but the signs are chosen randomly with equal probability for positive and negative sign. The perturbations are applied to all elements in parallel and the corresponding perturbed metric value $J_+^{(n)}$ is measured. Consecutively, perturbations are applied in the opposite directions and $J_-^{(n)}$ is measured, i. e.

$$J_\pm^{(n)} = J(u_1^{(n)} \pm \delta u_1, \ldots, u_j^{(n)} \pm \delta u_j, \ldots, u_N^{(n)} \pm \delta u_N) \tag{1}$$

The used metric perturbation is obtained as the difference of the two perturbed values:

$$\delta J^{(n)} = J_+^{(n)} - J_-^{(n)} \tag{2}$$

Finally the control voltages are updated according to the rule

$$u_j^{(n+1)} = u_j^{(n)} + \gamma\,\delta J^{(n)}\,\mathrm{sign}(\delta u_j)\ , \tag{3}$$

where γ is a gain factor scaling the size of the control voltage correction.

The AdOpt VLSI controller[4] implements major parts of the stochastic parallel gradient descent algorithm. Each AdOpt chip provides simultaneously 19 control voltages u_j and allows for a scaleable control system architecture. The chip comprises circuits for application and generation of pseudo-random perturbation voltages δu_j, for control signal update according to the control algorithm (3) and for preservation of the control parameter values u_j between subsequent iterations. Clocking signals, measurements of the metric signal and control of some system parameters are provided by a PC with digital and analog I/O boards. It also provides the sign of the metric change and an update pulse with a variable length proportional to $|\gamma\,\delta J^{(n)}|$ to the AdOpt chips, which performs updates using the full update term $\gamma\,\delta J^{(n)}\,\mathrm{sign}(\delta u_j)$ for each channel. In general, the PC may be replaced by a micro-controller but has advantage during search for appropriate system parameters and for data collection in an experimental stage.

3. ADAPTIVE LASER BEAM FOCUSING SYSTEM

The adaptive focusing system used is depicted in Fig. 1. The laser beam was reflected from the MEMS mirror and focused by the lens *L1* and the convergent beam was divided using beamsplitter *BS2*. A small pinhole (50 µm diameter) was placed in the first focal plane. The light power emergent from the pinhole was measured by a fast photodetector and was used as the system performance metric *J*, which is proportional to the Strehl ratio of the laser beam. An iris diaphragm *D* was placed in the second focal plane, which is imaged by the camera *CCD1* using beamsplitter *BS3* and lens *L2*. Images from the mirror surface were taken by camera *CCD2* using the imaging lens *L3*. Superposition with light from the reference mirror allowed to take interference pattern from the mirror surface. When cutting off higher diffraction orders with the iris diaphragm *D* the mirror was imaged with low resolution but allowed for a considerable phase contrast.

The MEMS deformable mirror used for this study was fabricated through conventional surface micromachining using polycrystalline silicon thin films. The 2 µm thick mirror membrane consists of 4×4 mirror segments with a side length of 250 µm each. The mirror elements are attached to a underlying 5×5 array of identical actuators via small posts (3 µm long). A single actuators consists of a 2 µm thick membrane with a span of 200 µm anchored to the substrate along two opposite edges (cf. Fig. 2). Application of an appropriate voltage deflects the actuator membrane, which is the top electrode of a parallel plate capacitor, due to electrostatic forces. With the deflection of the actuator the attachment post as well as the mirror membrane is moved. The hybrid type of mirror, which allows for piston as well as tip-tilt motion was realized by supporting the mirror segments at their corners, i. e. each post is attached to 4 segments.

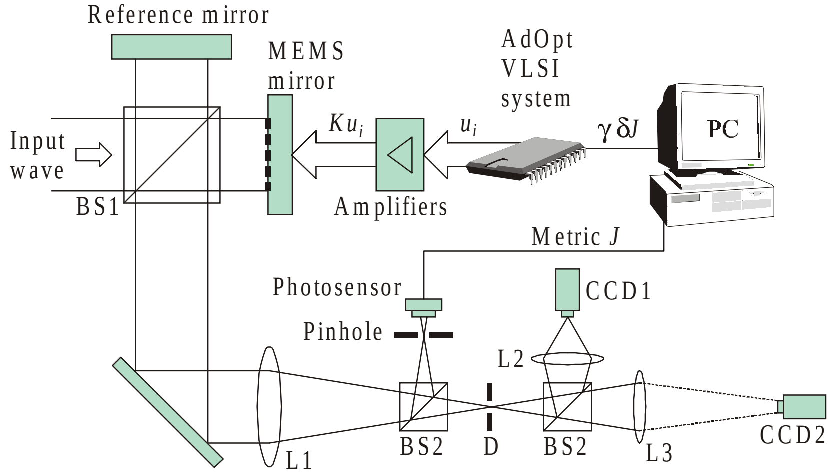

Figure 1. *Schematic of the adaptive laser beam focusing system*

The control voltages from the AdOpt chips in the range from -5 V to +5 V were not sufficient do drive the MEMS mirror actuators directly. Thus a set of high voltage amplifiers was used (26 amplifiers on one board), developed by Boston University for such capacitive loads as MEMS mirrors. They accept a 10 V range (with variable offset) as input and amplify it to the 0-300 V range required to control the actuators of the MEMS mirror.

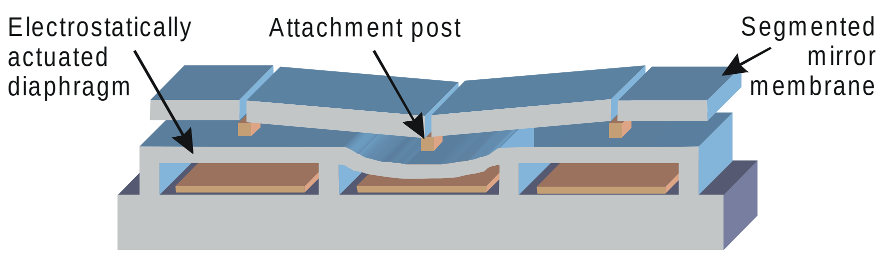

Figure 2. *Schematic of the segmented MEMS mirror with tip-tilt motion.*

4. MEMS DEFORMABLE MIRROR CHARACTERIZATION

In order to determine the dependence of the metric on the voltage of single mirror actuators the AdOpt VLSI system was replaced by a PC equipped with two 19 channel analog output boards, which allowed to control each channel individually. Sensitivity curves were measured varying the voltage of a single actuator from 0 V to 300 V while keeping all other actuators at 0 V. The results for four selected actuators are presented in Fig. 3. A common feature of all sensitivity curve is the existence of only one global maximum (at low voltages). Actuators 3 and 4, which move the tips of four mirror elements simultaneously have a higher impact on the metric J than actuators 2 and 1, moving two and one tip, respectively. Consecutive maximums or minimums are determined by a difference of one wavelength λ in the optical pathway, i. e. by $\lambda/2$ in actuator deflection. Maximums or minimums are not equidistant on a linear voltage scale, but reflect the approximately quadratic dependence of the deflection d_i of an actuator i on the voltage u_i, i. e. $d_i = K_i u_i^2$. Analyzing the voltages of maximums and minimums allows therefore to determine the deflection constant K_i of each actuator. As evident from Fig. 3 the deflection constants are not identical for all actuators. The observed phase shift (at λ = 690 nm) varies from about 5π to 6π, thus the corresponding shift in optical path length is between 1.7 and 2.1 µm.

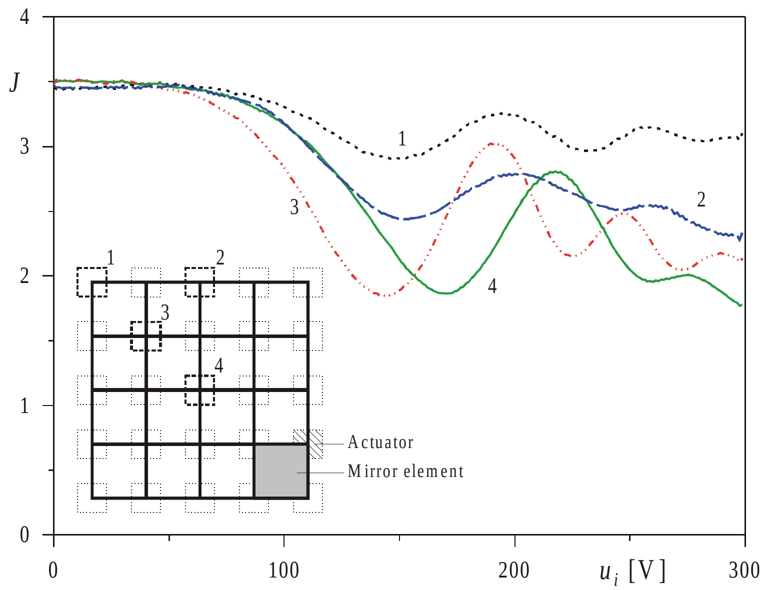

Figure 3. *Dependence of the system performance metric J on selected actuator voltages* u_i *. The location of the actuators within the MEMS mirror array is indicated in the inset.*

To measure the response characteristic of the MEMS mirror we used the laser beam focusing system as shown in Fig. 1, but connected about half of the actuator inputs (i. e. the inputs of the corresponding amplifiers) to a function generator. Application of an sinusoidal voltage induces an oscillating component of the metric *J*. To work in a linear regime, the amplitude of the input sine signal and a d.c. offset were chosen in such a way, that the induced metric change $\Delta J(\nu)$ was also nearly sinusoidal. Then the amplitude of $\Delta J(\nu)$ was measured in dependence on the frequency ν of the input sine signal. The result of this measurement is shown in Fig. 4. It demonstrates the high frequency capability of the MEMS mirror from Boston University. In the range up to about 10 kHz the amplitude $\Delta J(\nu)$ varied only slightly. At higher frequencies a significant drop-down of the signal was observed. In this range the signal amplitude $\Delta J(\nu)$ in the experiments is not only influenced by the mirror but also by the high voltage amplifier and the sensor. The amplifiers have a asymmetric behavior with a rise time of about 1.5 μs and a rise time of about 20 μs. An independent measurement of the amplifier characteristic was used to correct the measured data (corrected data are shown in Fig. 4). The sensor (photomultiplier with amplifier module) was not characterized in this frequency range but has a bandwidth of about 20 kHz according to manufacturer's specifications. Thus the mirror may have indeed a much higher operation frequency limit than the measurements as presented here imply.

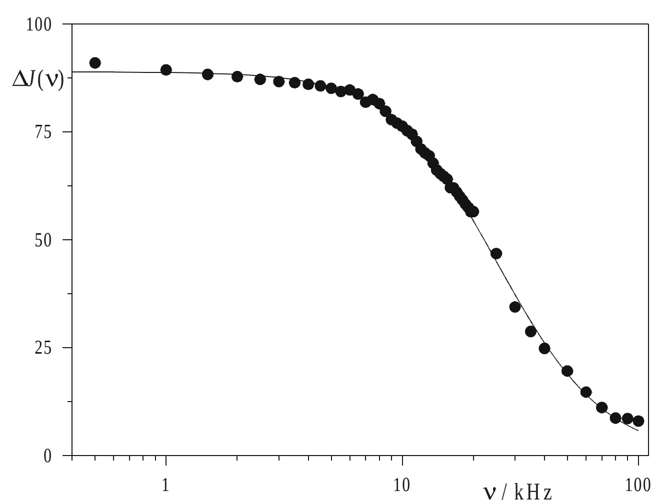

Figure 4. *Response characteristic in dependence on the frequency of the input signal of the 5×5 actuator tip-tilt motion MEMS mirror from Boston University*

5. PERFORMANCE OF THE CLOSED LOOP SYSTEM

The performance of the closed loop system implementing the Boston University MEMS mirror was studied with the set-up as depicted in Fig. 1. Two AdOpt chips were used in the electronic circuit to control the 25 mirror actuators. We did neither include a device to introduce wavefront distortion in the system nor was the incoming laser beam propagating through atmospheric turbulence. Instead the adaptation performance was evaluated by means of correction of self-induced aberrations.

Because the AdOpt system doesn't allow to control the voltages of the channels directly, aberrations were introduced using conditions, which forced the system to minimize the metric and therefore to apply quasi-random voltages to the mirror. In the experiments we performed consecutive minimization-maximization cycles with 4096 iterations each. During the first half of the cycle (iterations $n = 0$ to $n = 2047$) the update coefficient γ was chosen positive in order to minimize the metric, i. e. to introduce wavefront distortions into the system. At $n = 2048$ the sign of γ was changed and the maximization half-cycle was started, compensating the self-induced aberrations. After a cycle was finished the measured values of the metric $J^{(n)}$ and the metric perturbation $\delta J^{(n)}$ for each of the iteration steps n were saved. Typically 500 to 1000 cycles were performed for one particular experiment. After finishing the measurements the data of all consecutive trials were used to obtain average curves for the metric $< J^{(n)} >$ and metric perturbation $< \delta J^{(n)} >$ as well as to evaluate statistical data.

Fig. 5 presents images of the focal plane as well as interferograms of the MEMS mirror surface after minimization and maximization. The maximum status was almost identical with the condition, when 0 V was applied at all actuators. Only a very small deflection of the actuators at the edge was observed. The interference pattern of the maximum status shows also the aberration of the single mirror elements, the reason for a pronounced diffraction into higher orders. It is worth noting, that more recent mirror prototypes of Boston University have significantly improved surface quality. The mirror used for this study doesn't represent the technological achievement in this direction.

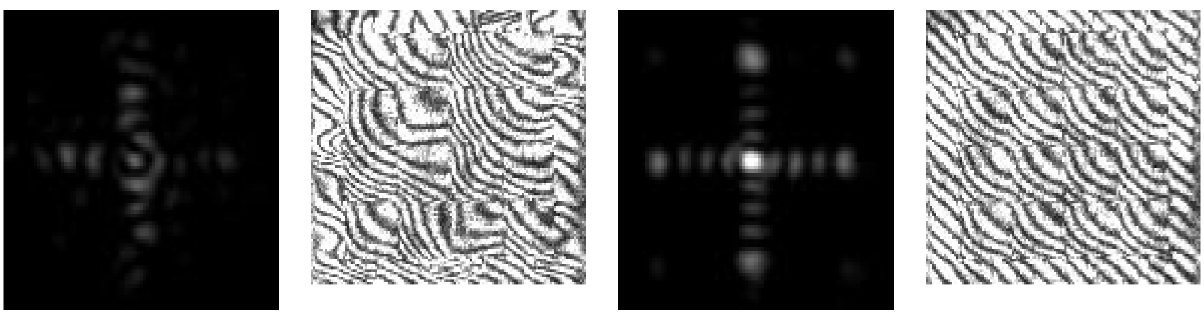

a **b**

Figure 5. *Focal plane images (left) and interference pattern (right) after minimization (a) and maximization (b), respectively.*

The results of a typical experiment as described above are presented in Fig. 6. The curve of the averaged metric J in dependence on the iteration step number n (Fig. 6a) demonstrates the fast convergence of the system. About 50 iterations were required to recover 80 % of the maximal value after minimization. The average minimization process was significantly slower. This may be understood considering the multistability of the system, which will be discussed below.

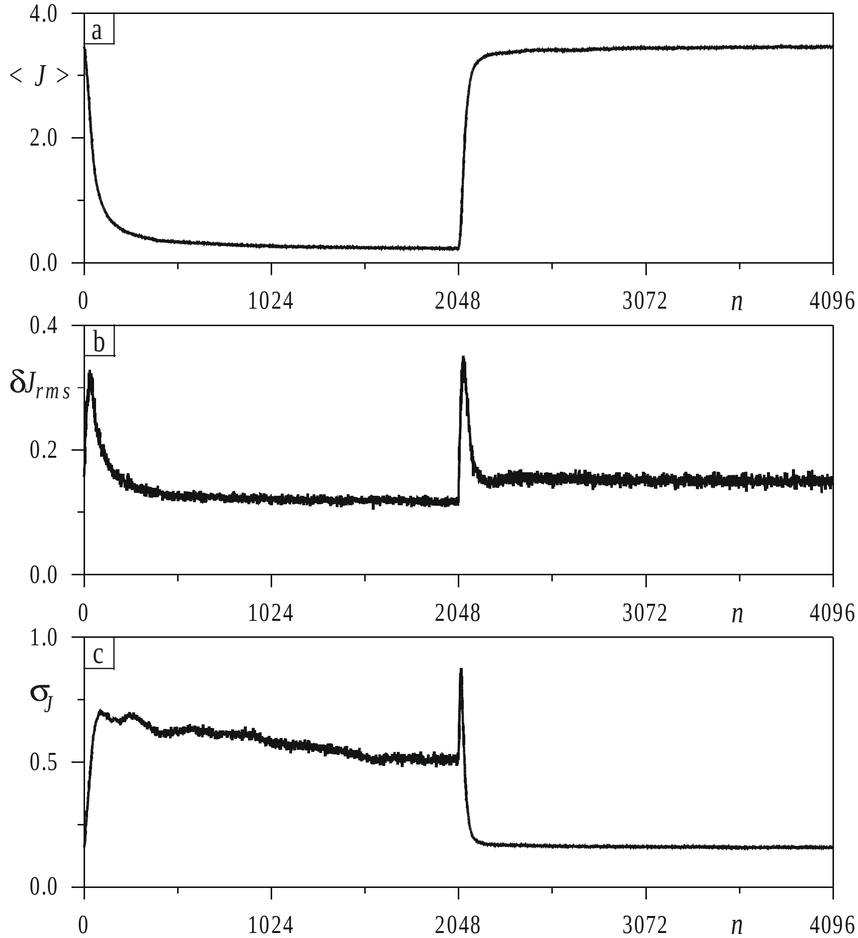

Figure 6. *a) Average of the metric* $< J >$ *during maximization-minimization cycles in dependence on iteration step number n; b) root mean square of the metric perturbation* $\delta J_{rms} =< \delta J^2 >^{1/2}$*; c) normalized standard deviation of the metric* $\sigma_J =< (J- < J >)^2 >^{1/2} / < J >$.

The adaptation speed of an laser focusing system may be characterized taking into account the number of iterations, which is required to achieve a certain percentage of the maximal value after minimization. However, this is not appropriate in general, because recovery from high self-induced aberrations (with very low or even zero *J* value) is a very unlikely task in adaptive optics systems and is difficult not only for the gradient descent algorithm. A better measure of performance is the maximum slope of the maximization curve $J'_{max} = (dJ / dn)_{max}$. However, for the true adaptation speed both the slope J'_{max} and the iteration rate $\dot{n} = dn / dt$ have to be considered. With the system used for the experiments a maximal iteration rate of $\dot{n} = 5900\,\mathrm{s}^{-1}$ was possible, limited by the speed of the PC (Pentium II processor at 450 MHz) and the I/O boards. Introducing appropriate delays in the control program allowed to reduce this rate to any lower value. A comparison of J'_{max} values achieved at different iteration rates from 500 to 5900 s^{-1} showed no decrease for higher $\dot{n}$ values. This is in accordance with the response measurements shown in Fig. 4, indicating only a small, negligible decrease of performance of the MEMS mirror in this frequency range.

The root mean square values of the measured metric perturbation are presented in Fig. 6b. Metric perturbations are higher during the transitions between *extrema* but are non-negligible even in maximum or minimum, where they should be zero in ideal case. This shows that the system is not in a steady state at *extremum* values but has a certain dynamics driven by noise present in the system and a minimum update voltage inherent to the AdOpt system. One should also consider, that noise (from the incoming laser beam power and the photosensor and its amplifier) contributes directly to the measured δJ value. It is typically proportional to the metric value *J* and the contribution is thus much higher to the maximum than to the minimum state. In the presented case the noise contribution in the maximum to the apparent δJ_{rms} value is about 0.05, that is almost 25 % and about the difference between δJ_{rms} in maximum and minimum.

In Fig. 6c the normalized standard deviation $\sigma_J^{(n)} =< (J^{(n)} - < J^{(n)} >)^2 >^{1/2} / < J^{(n)} >$ of the metric J is shown. As one may have expected, fluctuation are high during the transitions and in the minimum state, and lower in the maximum state. The absolute values however are quite high, about 0.2 in the maximum. This high value is induced by the multistability of the system. The system doesn't reach the global maximum in each maximization half-cycle, but may stop in a local maximum with lower J value. Such a local maximum corresponds e. g. to the second maximum of the sensitivity curves shown in Fig. 3. In order to analyze this behavior we evaluated the distribution of J values during the last 1000 iteration steps of the maximization as well as the minimization half-cycle. The number N of J values found within intervals of size 0.01 in dependence on J is presented in Fig. 7 (left side). Several well separated peaks were observed in the histogram of maximization as well as minimization. The right side of Fig. 7 shows images of the MEMS mirror surface for several different maximums. They were taken allowing only low order Fourier components to pass a spatial filter in the focal plane. The deflections are visible through diffraction contrast. The top left picture depicts the global maximum with all actuators at the same level. The other pictures show different numbers of deflected actuators corresponding to different local maximums.

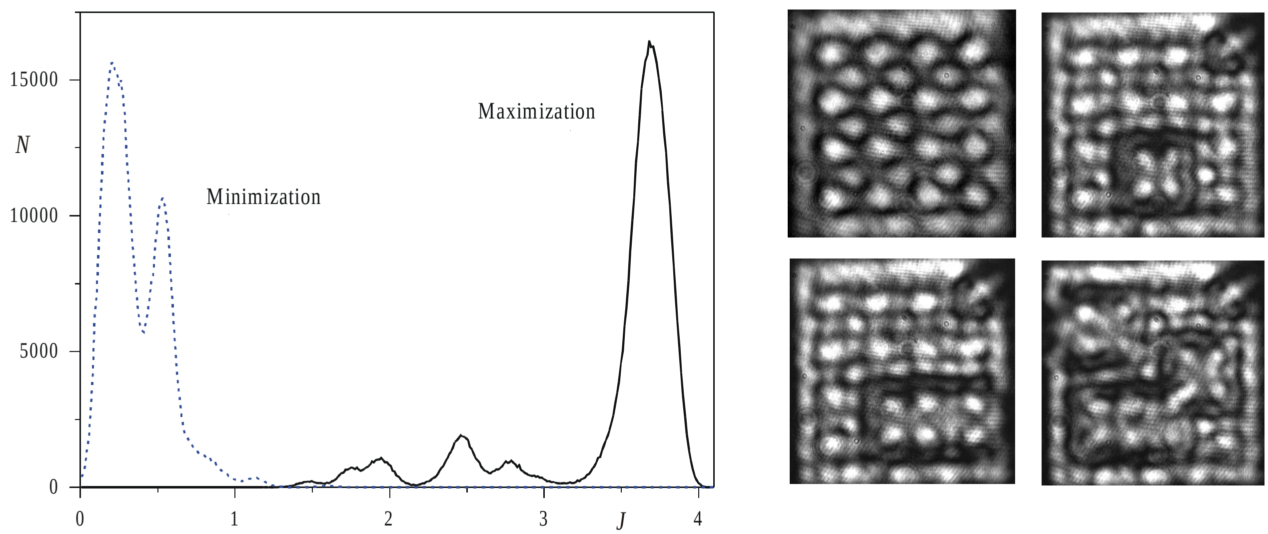

Figure 7. *Left: Distribution of J values during the last 1000 iteration steps of the minimization and maximization half-cycle. Data are taken from 500 runs. Right: Pictures of the MEMS mirror surface after maximization, showing the global maximum state (top left picture) and different local maximums.*

We observed a distinct difference in the multistability behavior in minimization and maximization. If the system finds a local maximum during maximization, it usually remains in that state. During minimization however, "hopping" between different local minimums until reaching the final value is much more likely. Evaluation curves, selected to demonstrate this behavior, are shown in Fig. 8. The reason for this different behavior is evident from the sensitivity curves (Fig. 3). The difference between maximum and minimum J values at low voltages (corresponding to the global maximum) is a large barrier, whereas the relative small difference at higher voltages (corresponding to the minimum) makes a transition from one state to another more likely.

This behavior explains also, why minimization in the average metric curve (Fig. 4a) appears slower than maximization. The absolute value of the maximal slope of an individual minimization evaluation curve is of the same order as of the maximization. In the average curve, however, the momentary staying at intermediate local minimum J values is summed up and the average slope becomes lower. In the maximization half-cycle, the system usually proceeds to one final maximum (whether local or global) and the average slope is thus more comparable to that of the curves for individual runs.

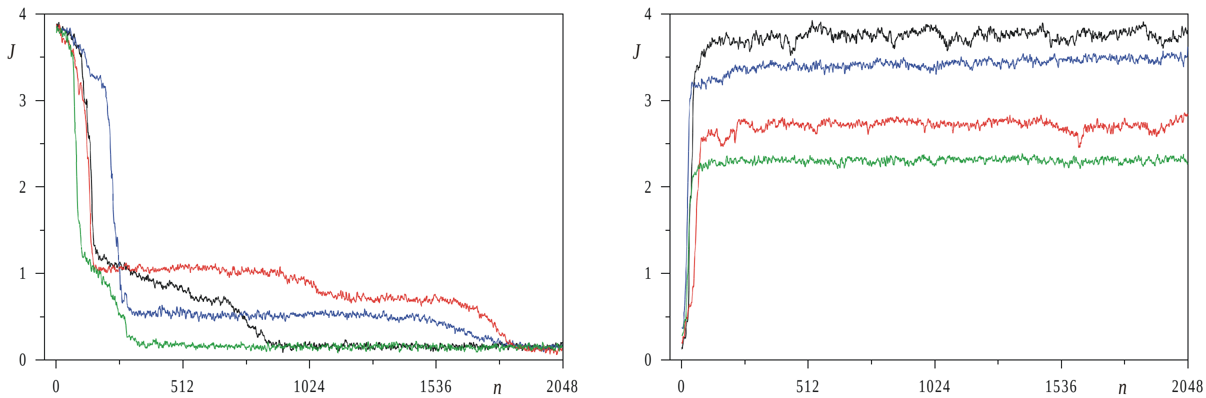

Figure 8. *Selected evaluation curves for minimization (left) and maximization (right), demonstrating different probabilities for "hopping" between extrema.*

6. ADAPTIVE UPDATE GAIN CONTROL ALGORITHM

The iteration algorithm (equation 3) allows for the free choice of the update gain parameter γ. Evidently, a too small γ will allow only for slow adaptation. On the other hand, a too high γ makes overshooting more likely and thus also slows down adaptation speed. In order to find an optimal γ value we studied therefore systematically the performance of the system in dependence on the chosen γ value. In Fig. 9 (left side) the adaptation speed represented by the maximal slope J'_{max} of the maximization curve is presented. The graph doesn't show a maximum or saturation at the chosen γ values and would, without further knowledge, indicate that the optimal value should be higher. However, a higher γ destabilizes the system and leads to a large variance when an *extremum* has been reached. This is demonstrated in the right side of Fig. 9, where the J value distribution during the last 1000 iteration steps for maximization for three different γ values is shown. With increasing γ the peak for the global maximum became broader and was shifted to lower values. Consequently, the average value $< J >$ and thus the Strehl ratio was decreased. It's worth noting, that (though difficult to see from Fig. 9 because of a very low number of counts N in that range) the highest measured value for each curve is almost the same.

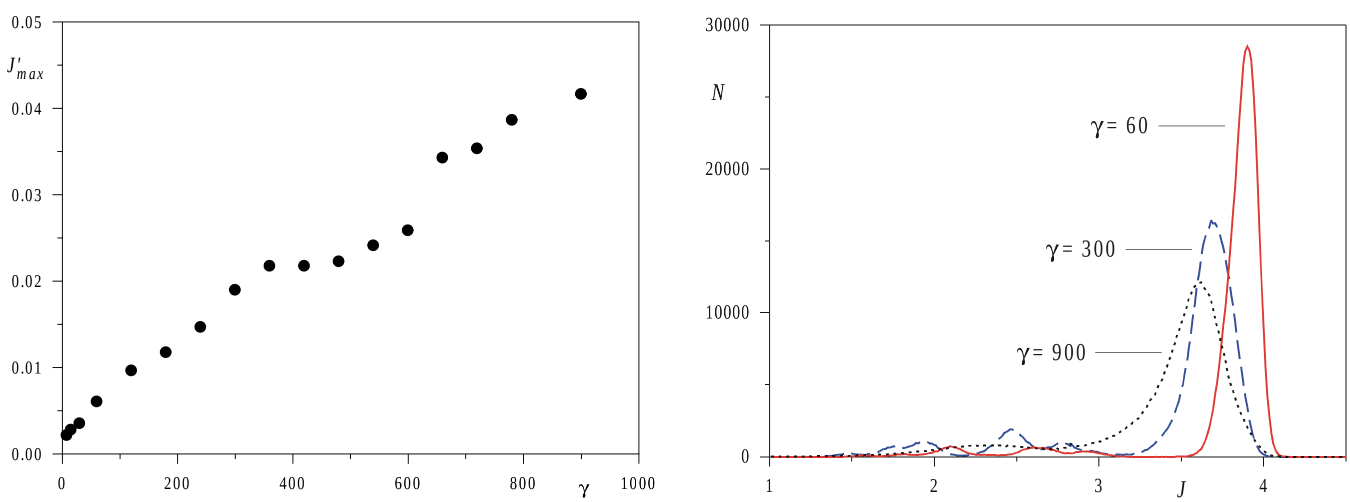

Figure 9. *Left: Dependence of the maximal slope J'_{max} (normalized to the maximum J value) on γ. Right: Histograms for J values during the last 1000 iteration steps in a maximization half-cycle for three different update gain parameters γ.*

The problem of the trade-off between convergence speed and average maximum value can't be overcome using the algorithm as presented in equation 3 with a fixed γ value. One possible solution is to use an algorithm, which implements a self-optimization of γ, i. e. which chooses a large γ value, in the case that the system needs significant large changes of the control voltages in order to optimize, and a small γ value when an *extremum* was found in order to have a small variance.

Our approach to implement such a self-optimizing algorithm based on the idea that the γ value which is used in a particular iteration step should be close to a pre-chosen value γ_0 in the case of quasi-steady-state condition at an *extremum*. If considerable corrections are required, the γ value should increase significantly. This was realized using the iteration algorithm

$$\gamma^{(n+1)} = (1-\alpha)\,\gamma^{(n)} + \alpha\,\gamma_0 \left[1 + f\,H^{(n)}\right], \tag{4}$$

where α is an update coefficient for γ and $H^{(n)}$ is a function, which represents the actual situation, i. e. it should take high values if large changes of the actuator voltages are required and low values in the other case. The linear scaling factor *f* is required to adjust the value for γ corrections to an appropriate magnitude depending on the chosen function $H^{(n)}$. The main problem is to find an appropriate expression for $H^{(n)}$. One approach, discussed earlier by Carhart et al.[6], considers the sign of the two metric perturbations δJ_+ and δJ_-: If the system is in an *extremum* state, one expects equal signs for both perturbations. For instance, in the maximum both values should be negative, because a lower *J* value will be measured for perturbation in either direction. On the other hand, if the system is not in an *extremum*, one expects, in general, different signs for δJ_+ and δJ_-. Thus one may formulate a criterion as

$$H_1^{(n)} = |\mathrm{sign}(\delta J_+^{(n)}) - \mathrm{sign}(\delta J_-^{(n)})|\ , \tag{5}$$

However, in our experiments we found that this criterion was not sufficient in presence of reasonable noise. A second approach used the fact, that the absolute values of metric perturbations at *extrema* are smaller than in the case where the system needs to perform large corrections (cf. Fig. 5b). Thus one might use

$$H_2^{(n)} = |\delta J^{(n)}| \tag{6}$$

A third approach takes care about whether updates do really change significantly the metric value, i. e. the current $J^{(n)}$ value is compared with that of an earlier iteration step $J^{(n-a)}$. The difference should be small in an *extremum* but larger for real adaptation:

$$H_3^{(n)} = -\mathrm{sign}(\gamma_0)[J^{(n)} - J^{(n-a)}] \tag{7}$$

Here *a* is the difference in the iteration number for the comparison of the *J* values. It is reasonable to choose it approximately as large as the inverse of the update coefficient α (i. e. $a \approx 1/\alpha$) in order to have similar time scales for averaging and comparison. The sign of γ_0 is considered to allow for both maximization and minimization of the metric. By convention, negative γ are used for optimization, thus the minus sign is required.

Neither of the three discussed approaches H_1, H_2, H_3 provided a sufficient improvement of the algorithm. However, the product of three different terms

$$H^{(n)} = H_1^{(n)}\ H_2^{(n)}\ H_3^{(n)}\ , \tag{8}$$

was found to be successful. In general, the current γ value should depend not only on the properties of the very recent iteration step, but should consider an average of several recent iterations. In some sense, this is already considered in equation 4, where the current γ value is obtained as the weighted average of $\gamma_0[1 + H^{(n)}]$ (more recent iterations contribute stronger) and α controls quasi the number of considered iterations (the smaller α, the more iterations). However, the values of $H^{(n)}$ may vary strongly from one iteration to the next and thus allowing for considerable variances in γ and consequently also in the metric *J*. An improvement of the situation was possible introducing an additional averaging for $H^{(n)}$, i. e.

$$H^{(n)} = (1-\alpha)\, H^{(n-1)} + \alpha\, H_1^{(n)} H_2^{(n)} H_3^{(n)} \;. \tag{9}$$

Fig. 10a shows the averaged metric evaluation curve of an experiment using the self-optimizing algorithm according to equations 4-7 and 9 with $\gamma_0 = 180$ and $\alpha = 0.2$ in comparison to the curve obtained with a fixed value $\gamma = 180$. In Fig. 10b the averaged adaptive γ value is presented. The curve demonstrate, that the chosen algorithm indeed controls γ in an appropriate way. In the minimum or maximum quasi-steady-state γ is approximately equal to the chosen value $\gamma_0 = 180$, whereas in the transition to the maximum values higher than 1000 are obtained. Maximization as well as minimization with adaptive gain are faster than with a fixed γ. As visible from the insert of Fig. 10a, the maximal slope J'_{max} for maximization was improved by about 50 %.

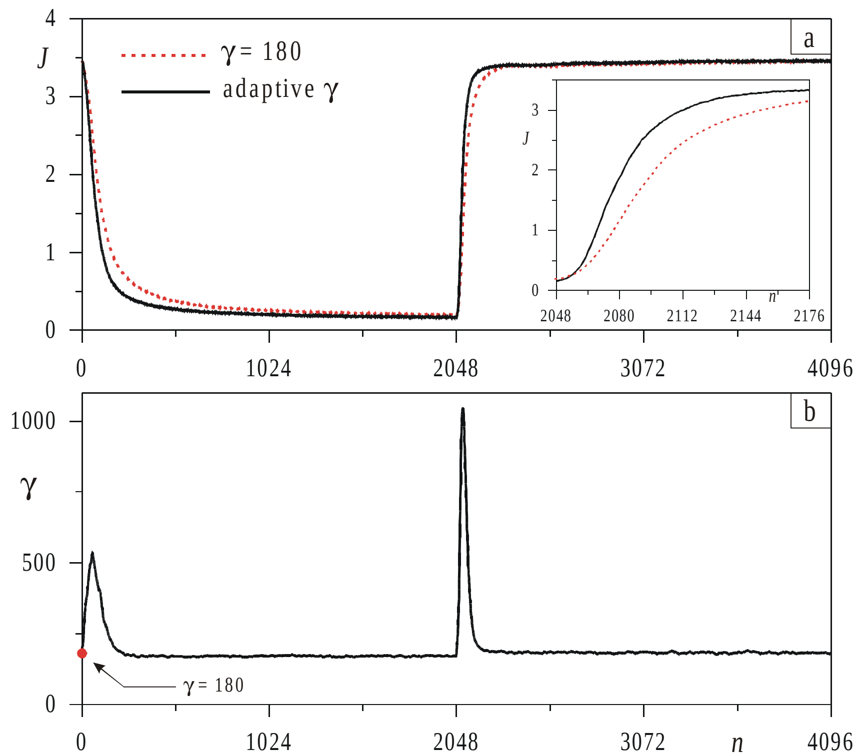

Figure 10. *a) Comparison of minimization-maximization evaluation curves using algorithms with adaptive and with constant update gain parameter γ. b) Averaged adaptive γ values during the maximization-minimization cycles.*

7. CONCLUSION

An adaptive laser beam focusing system based on a MEMS deformable mirror and VLSI controller implementing a stochastic parallel gradient-descent algorithm with an iteration rate of almost 6000 s^{-1} was presented. Because the rate was limited by the computer equipment used to complete the closed-loop system but not by the MEMS mirror or the VLSI controller, a further enhancement of the iteration rate with improved equipment must be expected. It was also shown, that a modification of the update rule, implementing a self-optimization of the update gain parameter, enhanced the adaptation speed by about 50 %. This offers the perspective that a major drawback of model-free optimization strategies, namely a so far not sufficient bandwidth for corrections of fast atmospheric turbulence induced wavefront distortions due to the requirement of a higher number of iteration steps, may be overcome using already existing or currently developed high bandwidth MEMS mirrors and VLSI controllers.

ACKNOWLEDGMENT

This work was performed at ARL's Intelligent Optics Laboratory in Adelphi, MD, in frames of a cooperation project with the New Mexico State University with financial support by the Air Force Office of Scientific Research (contract number F49620-99-1-0342) The authors would like to thank Gary W. Carhart for developing computer software used for the presented experiments and Marc Cohen for assistance with the AdOpt VLSI controller circuit.

REFERENCES

1. R. K. Tyson, *Principles of Adaptive Optics*, 2nd edition (Academic, Boston, 1997).
2. M. A. Vorontsov, G. W. Carhart, and J. C. Ricklin, "Adaptive phase-distortion correction based on parallel gradient-descent optimization", *Opt. Lett.*, **22**, 907-909 (1997).
3. M. A. Vorontsov and V. P. Sivokon, "Stochastic parallel gradient descent technique for high-resolution wavefront phase distortion correction", *J. Opt. Soc. Am. A,* **15**, 2745-2758 (1998).
4. R. T. Edwards, M. Cohen, G. Cauwenberghs, M. A. Vorontsov, G. W. Carhart, "Analog VLSI Parallel Stochastic Optimization for Adaptive Optics", in *Learning on Silicon*, eds. G. Cauwenberghs, M. A. Bayoumi, (Kluwer Academic Publishers, Boston, Dordtrecht, London, 1999), Chapter 16, pp. 359-382.
5. A. Vorontsov, G. W. Carhart, M. Cohen, and G. Cauwenberghs, "Adaptive optics based on analog parallel stochastic optimization: analysis and experimental demonstration", *J. Opt. Soc. Am. A* (August 2000).
6. G. W. Carhart, M. A. Vorontsov, M. Cohen, G. Cauwenberghs, and R. T. Edwards, "Adaptive wavefront correction using a VLSI implementation of the parallel gradient descent algorithm", *Proc. SPIE*, **3760**, 61-66 (1999).